Journal of Fluids and Structures (2002) **16**(2), 153–173
doi:10.1006/jfls.2001.0408, available online at http://www.idealibrary.com on IDEAL®

DYNAMICS OF AN IN-LINE TUBE ARRAY SUBJECTED TO STEAM–WATER CROSS-FLOW. PART III: FLUIDELASTIC INSTABILITY TESTS AND COMPARISON WITH THEORY

K. Hirota, T. Nakamura and J. Kasahara

Mitsubishi Heavy Industries, Ltd., Takasago R & D Center, 2-1-1 Arai-cho Shinhama Takasago, Hyogo, Japan

N. W. Mureithi

Department of Mechanical Engineering, Kobe University Rokkodai 1-1 Nada-ku, Kobe Japan

T. Kusakabe

Mitsubishi Heavy Industries, Ltd., Kobe Shipyard and Machinery Works 1-1 Wadasaki-cho 1-chome, Hyogo-ku, Kobe, Japan

H. Takamatsu

The Kansai Electric Power Co., Inc. 3-3-22, Nakanoshima, Kita-ku Osaka, Japan

(Received 28 October 1999, and in final form 22 May 2001)

This paper presents the results of comprehensive flow-induced vibration tests conducted on an in-line array in steam–water two-phase flow. The responses of three essentially isolated flexible cylinders at different depths within the array were simultaneously measured. The main test parameters were, ambient pressure (and saturation temperature), in the range 0·5–5·8 MPa, void fraction, 0·70–0·96, and phase flow velocity. Tests reported here were conducted simultaneously with the damping tests reported in Part I of this study. At the highest pressures (3·0 and 5·8 MPa), strong instabilities, in homogeneous flow akin to single-phase flow occurred. The test tube located in the central region of the array was the most susceptible to instability. This was attributed partly to reduced two-phase damping deep in the array, while differences in local fluid forces at different locations in the array are not ruled out. The flow at 0·5 MPa was a nonhomogeneous intermittent slug-type flow. Strong turbulence excitation obscured clear fluidelastic instability; intermittent instability was, however, ascertained. Stability boundary calculations were done using unsteady fluid forces presented in Part II of this series of papers. Results for the case of $P = 5{\cdot}8$ MPa show good agreement with the measured instability boundary.

1. INTRODUCTION

Compared to the case of single-phase flow, fluidelastic instability in two-phase flow is dependent on a larger number of parameters. The roles played by quantities such as density, viscosity and flow velocity, which are well defined for single-phase flow, often become unclear in two-phase flow. Indeed, defining true independent flow parameters remains elusive as discussed for instance by de Langre *et al.* (1995) and as well demonstrated in Part II of this study (Mureithi *et al.* 2002).

0889–9746/02/020153 + 21 $35.00/0

The available data on vibration in two-phase flow is mainly from tests conducted using air–water mixtures. Air–water tests at atmospheric conditions are cost effective, hence their prevalence. The existence of fluidelastic instability in two-phase flow has been confirmed by several investigators, initially in tests employing air–water mixtures (Pettigrew & Gorman 1973; Heilker & Vincent 1981; Remy 1982; Nakamura *et al.* 1995; Pettigrew *et al.* 1989). The applicability of air–water results to prototypical steam–water conditions has some limitations. The mass ratio between the liquid and gas phases is much smaller in air–water than in steam–water. As a result, the slip ratios between the phases are different for the two mixtures (Feenstra *et al.* 1995). The flow regime transition boundaries are also not identical as is evident in the work of Feenstra *et al.* (1995). This may be important in cases where these boundaries are near or coincide with fluidelastic instability boundaries. For in-line arrays, for instance, Axisa *et al.* (1985) found that the stability boundary in steam-water flow was independent of the mass-damping parameter, being given by $U_c/fD = 5$. In the same parameter range, Pettigrew *et al.* (1989) found that in air–water flow, $U_c/fD = 4\sqrt{m\delta/\rho D^2}$ was a close approximation to the stability boundary, which they recommended as a design guideline.

A closer approximation to steam–water flow, at significantly reduced cost, is provided by freon two-phase flow. The fluid density ratio can be correctly scaled, while surface tension,

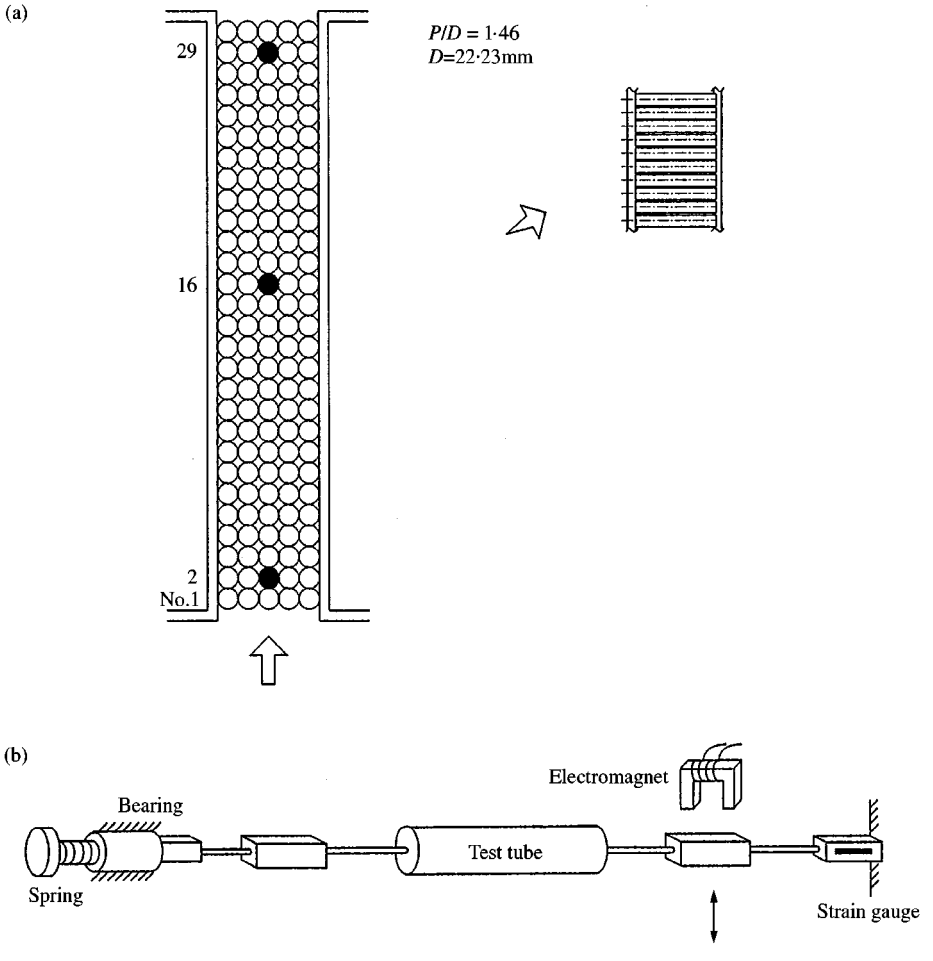

Figure 1. (a) The in-line test geometry and (b) flexibly supported cylinder.

another important parameter, is closely approximated. Freon tests have been carried out by several researchers. Pettigrew *et al.* (1995) and Feenstra *et al.* (1995) tested single-component freon two-phase flow. Test results showed considerable deviations from air–water tests. Pettigrew *et al.* (1995) reported a large drop in the instability velocity at high void fraction for freon flow. Gay *et al.* (1988) tested a triangular array in freon–water and air–water two-phase mixtures. While scaled tests unquestionably provide valuable information and data, important differences with prototypical conditions remain. The available data on fluidelastic instability in steam–water flow, corresponding to prototypical steam generator operating conditions, remains limited [see Axisa *et al.* (1985), Nakamura *et al.* (1995)].

In this paper, we present the results of vibration tests conducted simultaneously with the damping tests [reported in Part I, Nakamura *et al.* (2002)]. Test tubes were located in rows 2, 16 and 29 as indicated in Figure 1. Considering the large (row) separation between the test tubes, each tube could be considered as an isolated single flexible tube surrounded by rigid tubes. Data presented includes variation of response amplitudes and frequencies with flow velocity.

Unsteady fluid-force data for the highest pressure condition [see Part II, Mureithi *et al.* (2002)] are also employed in a stability analysis. As it becomes clear, the application of the measured fluid forces is far less straightforward than in the case of single-phase flow.

There has been limited theoretical analysis for the prediction of fluidelastic instability in two-phase flow. Nakamura *et al.* (1995) proposed two theoretical models for stability-boundary prediction for the homogeneous and intermittent flow regimes, respectively. An interesting concept was introduced in which spatial distribution of liquid and gas phases was replaced by an equivalent temporal distribution. The instability boundary was marked by the condition of net positive energy input to the tube from the flow. Marn & Catton (1992) modified the vorticity transport equation to account for two coexisting fluid phases. Numerical solutions were obtained using a finite-difference algorithm. Very reasonable agreement with experimental data was obtained. In the present work an unsteady fluid-dynamic model is considered (Tanaka & Takahara 1981; Chen 1983).

The main aspects of this work were reported in Hirota *et al.* (1996).

2. TEST MODEL AND EXPERIMENTAL PROCEDURE

The steam–water test loop is described in Part I of the series (Nakamura *et al.* 2002). A U-tube heat exchanger rated at 2 MW generates steam–water two-phase flow at a maximum pressure of 6 MPa and a temperature of 273°C. Flow velocity ranges are 0·0–1·0 m/s (liquid) and 4·5–12·0 m/s (vapour). Flow velocities are computed from mass flow rate measurements. The maximum uncertainty in the mass flow rate measurements is 5%. Void fractions from 0·5 to 1·0 can be attained within the test-section. The tube array is oriented as shown in Figure 1(a), so that fluid flows vertically upward against gravity.

The square geometry array consists of 30 tube rows with five tubes per row. The intertube pitch-to-diameter ratio is $P/D = 1{\cdot}46$ where $D = 22{\cdot}23$ mm. The three test tubes, having a mass of 0·96 kg/m, are flexibly mounted as depicted in Figure 1(b). To counter thermal expansion effects, one end of the flexible tube support has a sliding linear bearing support; a preloaded spring takes up the resulting slack. The three test tubes had a nominal natural frequency of 22 Hz and damping ratio in the range 0·29–0·45% in air. Specific values for each tube are shown in Table 1.

Parameters varied in the tests were ambient pressure (and temperature), void fraction and flow velocity. At each pressure and void fraction, the flow velocity was incremented from a low value (typically 1·0 m/s, average homogeneous velocity) until instability occurred or the maximum possible velocity was attained.

TABLE 1
Test tube frequency and damping at atmospheric conditions

Tube & direction	Air		Water ($P = 0{\cdot}1$ MPa, 20°C)		
	Frequency (Hz)	Damping (ζ_s %)	Frequency (Hz)	Damping	
				Total (ζ_t %)	Fluid-induced ($\zeta = \zeta_t - \zeta_s$) %
S29D	21·7	0·29	17·6	0·91	0·63
S29L	21·8	0·30	17·7	0·91	0·62
S16D	22·0	0·32	17·8	0·91	0·59
S16L	22·1	0·40	17·9	0·98	0·59
S2D	21·8	0·40	17·6	1·04	0·65
S2L	21·8	0·45	17·5	1·14	0·69

TABLE 2
Test parameters

Pressure/Temp. (MPa)/(°C)	Liquid velocity j_l (m/s)	Gas velocity j_s (m/s)	Superficial void fraction β
0·1/25	0·00–1·00	—	0·0
0·5/150	0·13–1·10	1·2–10·0	0·9
3·0/230	0·10–0·72	0·9– 7·0	0·9
5·8/273	0·00–1·00	—	0·0
	0·10–1·33	0·9– 3·5	0·7, 0·8, 0·9, 0·96

For $P = 5{\cdot}8$ MPa, tests were conducted at four void fraction values. The test conditions and parameter ranges are summarized in Table 2. Results of thermal hydraulic flow pattern measurements may be found in the Appendix in Part I of the series (Nakamura *et al.* 2002). For reference purposes, a test in single-phase flow was also conducted.

3. TEST RESULTS

3.1. DEFINITION OF TWO-PHASE FLOW PARAMETERS

Homogeneous parameters are used to present all data, unless otherwise specified. Orifice plates at the respective steam and water outlets measure the mass flow rates, W_g and W_l. The corresponding average phase velocities are

$$j_l = \frac{W_l}{\rho_l A}, \quad j_g = \frac{W_g}{\rho_g A}, \tag{1}$$

respectively, for water and steam. ρ_l, ρ_g are liquid and vapour densities, respectively. Equation (1) gives *gap* velocities since the area A is the gap flow area. From equation (1) the average homogeneous flow velocity is

$$U = j_g + j_l. \tag{2}$$

The homogeneous void fraction is

$$\beta = \frac{j_g}{j_g + j_l}. \tag{3}$$

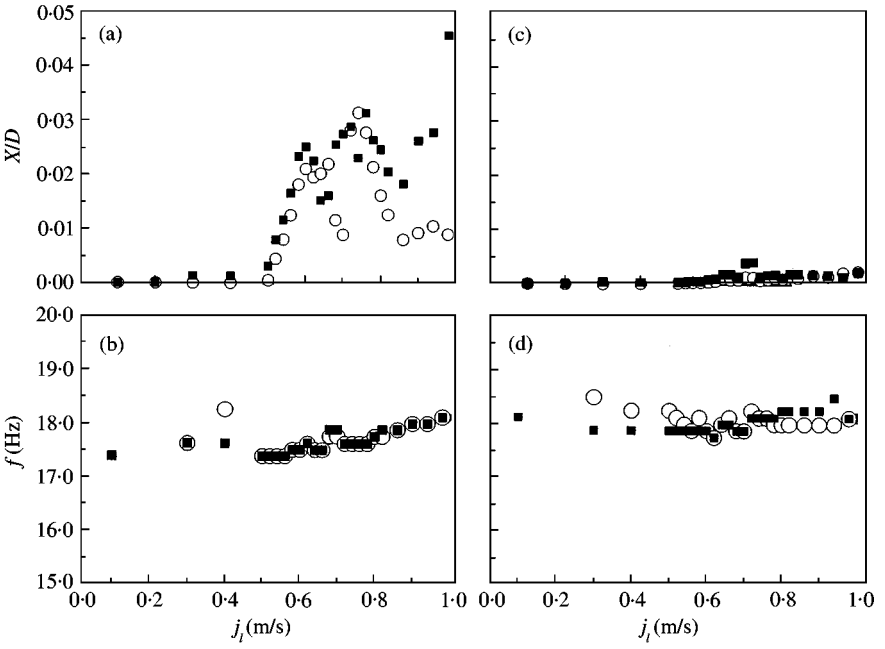

Figure 2. (a, c) Tube vibration amplitudes and (b, d) frequencies; (a, b) for tube S2; (c, d) for tube S16; in water flow for $P = 0{\cdot}1$ MPa, $T = 20°C$; ■, drag; ○, lift.

Using this definition of void fraction, the following homogeneous density may be defined:

$$\rho = \rho_g \beta + \rho_l (1 - \beta). \tag{4}$$

From equations (2) and (4), the reduced velocity and mass damping parameter are U/fD and $m\delta/\rho D^2$, respectively. Connors' constant is given by

$$K = \frac{U_c/fD}{(m\delta/\rho D^2)^{1/2}}, \tag{5}$$

where δ includes structural and total fluid damping, and m is the sum of the structural mass (0·96 kg/m) and the fluid added mass.

3.2. Vibration Tests in Water Flow

In this set of tests the gap flow velocity was varied in the range $0{\cdot}1 < j_l < 1{\cdot}0$ m/s, at atmospheric pressure, $P = 0{\cdot}1$ MPa. Tube r.m.s. vibration amplitudes were determined from response auto-spectra in steady flow at each velocity setting. There is little tube vibration for $j_l < 0{\cdot}50$ m/s as seen in Figure 2 where r.m.s. amplitudes, normalized with the tube diameter, are plotted versus j_l for the second-row tube (S2). The low response amplitudes are attributed to low turbulence level.

Two peaks in the tube response are observed in Figure 2(a) at 0·60 and 0·75 m/s. Previous studies have shown that the present array is susceptible to flow periodicity resonances. The Strouhal numbers corresponding to the two maxima are $S_1 = 0{\cdot}65$ and $S_2 = 0{\cdot}51$. In a combined flow visualization and vibration study Weaver & Abd Rabbo (1985) obtained a Strouhal number $S_w = 0{\cdot}60$ for a slightly wider array ($P/D = 1{\cdot}5$); S_w was found to be associated with symmetric vortex shedding which was synchronized along tube columns.

This is the mechanism associated with S_1 in the present tests. The slightly higher value than S_w above is due to the smaller array spacing here ($P/D = 1{\cdot}46$) compared to $P/D = 1{\cdot}5$ in Weaver & Abd Rabbo's study. Ziada & Oengoren (1992) have shown that, unlike the case of a solitary cylinder, symmetric wake shedding within in-line arrays is the result of symmetric jet instability in the flow lanes. Weaver & Abd Rabbo (1985) did not report a second Strouhal number in their tests. It is possible that fluidelastic instability (of their multiply flexible array) may have pre-empted the manifestation of a second flow periodicity mechanism. Ziada & Oengören (1992) did report as many as three Strouhal numbers, 0·92, 0·65 and 0·46, for a rectangular array with spacing 1·35D and 1·6D in the cross-flow and in-flow directions, respectively; $S = 0{\cdot}92$ was related to symmetric jet instability and $S = 0{\cdot}65$ associated with an asymmetric jet instability. The ratio between the latter Strouhal number and the symmetric instability Strouhal number was 0·7. In the present tests $S_2/S_1 = 0{\cdot}78$. The difference in Strouhal number values and slight difference in ratios here might be attributed to array differences.

Evidently the oscillatory mechanisms above are only present in the array entrance region. Deep in the array they are not manifested; hence, tubes S16 and S29 are only excited by turbulence. Response amplitude and frequencies for tube S16 are shown in Figure 2(c,d); tube S29 had a very similar response.

The second-row tube was found to undergo fluidelastic instability in the in-flow direction at a higher flow velocity. The critical velocity is estimated to be 0·75 m/s by an extrapolation of the amplitude growth curve. For all the tubes, the response frequency shows an overall increase with flow velocity. The maximum increase is 0·8 Hz in the drag direction.

Figure 3 shows the results at $P = 5{\cdot}8$ MPa for the second-row tube in water flow. While in the 0·1 MPa test the tube undergoes flow-periodicity excitation followed by fluidelastic instability, these phenomena are not observed at 5·8 MPa for the same flow velocity range. In-flow and cross-flow frequencies also undergo no lock-in. Note, however, that for $j_l > 1{\cdot}0$ m/s an increasing trend in the response amplitude is apparent, suggesting the occurrence of fluidelastic instability near 1·0 m/s.

The lack of flow-periodicity excitation at high pressure is rather surprising. We note, however, that the Reynolds number is roughly one order of magnitude higher at 5·8 MPa than at 0·1 MPa. Flow periodicity is strongly dependent on Reynolds number. For a solitary cylinder in cross-flow, the range $3 \times 10^5 < \mathrm{Re} < 3{\cdot}5 \times 10^6$ is a critical transition region in which regular vortex shedding does not occur (Chen 1987, p. 250). Clearly, the identical numerical values will not apply for a tube array. It is noted, however, that for $P = 5{\cdot}8$ MPa,

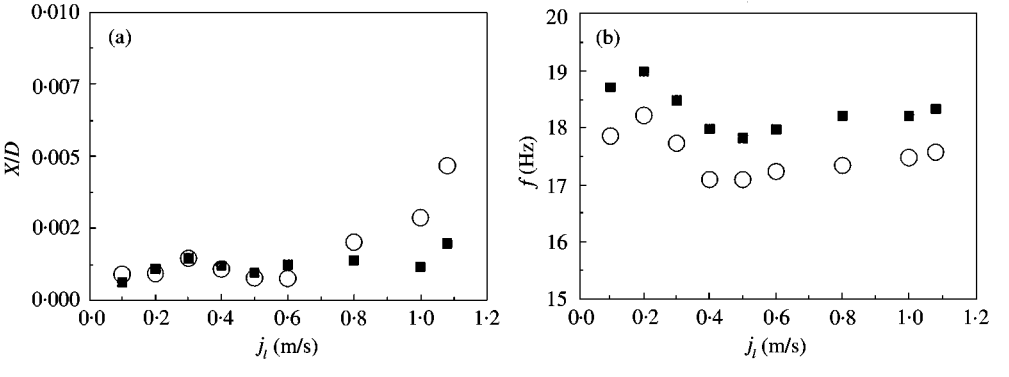

Figure 3. (a) Tube S2 response amplitudes and (b) frequencies in water flow for $P = 5{\cdot}8$ MPa, $T = 273°C$; ■, drag; ○, lift.

the flow velocity range $0.60 < j_l < 1{\cdot}2$ m/s corresponds to the Reynolds number range $10^5 < \mathrm{Re} < 2 \times 10^5$, while for $P = 0{\cdot}1$ MPa, the range is $1{\cdot}3 \times 10^4 < \mathrm{Re} < 2{\cdot}6 \times 10^4$. The latter falls within the Re range for strong vortex shedding behind a solitary cylinder. It would therefore appear that a Reynolds number effect may, at least partially, explain the lack of organized flow periodicity for 5·8 MPa.

3.3. Tube Vibration in Two-Phase Flow for $P = 0{\cdot}5$ MPa, $T = 150^\circ$C, $\beta = 0{\cdot}90$

In this test, the homogeneous flow velocity $U(= j_g + j_l)$ was varied from 1 to 10 m/s. Both j_g and j_l were simultaneously varied to maintain a void fraction of 0·90 throughout the test. Figure 4 shows the tube response and frequencies. All three tubes showed increasing tube response in the lift direction. Drag-direction response, on the other hand, remained almost unchanged at an average value $0{\cdot}01D$; an increasing trend is, however, discernible for tube S16, while it is very low for S2 and S29. The increasing cross-flow response with flow velocity suggests the occurrence of an instability. From Figure 4, however, it is not obvious what the instability critical velocity value should be. This is attributed to the high turbulence level associated with the flow type for this pressure. Note that at the lowest test velocity, the r.m.s. tube response is $0{\cdot}005D$. The critical instability velocity was estimated from the variation of cross-flow tube damping level with flow velocity. The critical velocities for tubes S2, S16 and S29 were estimated to be 4·5, 3·0 and 6·5 m/s, respectively. The strong turbulence excitation makes these estimates significantly error-prone. Instability velocity estimates were based not only on tube response amplitude variation but also changes in apparent tube damping. It was shown in Part II of the series (Mureithi *et al.* 2002) that the unsteady fluid forces are nonstationary for $P = 0{\cdot}5$ MPa. A time frequency analysis confirmed that instability, when it occurs, will at best be intermittent. The vibration results support this assertion. For all the tubes, the response frequencies showed a slight increase as flow velocity increased; this may partly be attributed to steady drag. There was almost no coupling between the in-flow and cross-flow motions, even after instability (except possibly for tube S16). This is again attributed to the high turbulence level associated with the nonhomogeneous flow at this pressure.

3.4. Tube Vibration in Two-Phase Flow for $P = 3{\cdot}0$ MPa, $T = 230^\circ$C, $\beta = 0{\cdot}90$

The homogeneous flow velocity could be varied in the range $0 < U < 8$ m/s. Figure 5 shows tube response amplitudes and frequencies. All three test tubes show clear fluidelastic instability in this test. The critical velocities are 4·8, 3·2 and 3·0 m/s, respectively, for tubes S2, S16 and S29. Hence the second-row tube is marginally stable compared to the other two tubes. Instability causes coupling between the in-flow and cross-flow motions, as seen in the frequency plots. In-flow vibration amplitudes, however, remain relatively small. It is evident that the tube responses are markedly similar to the response in single-phase flow. At this pressure and void fraction, the flow is essentially homogeneous, bubbly or froth flow.

3.5. Test in Two-Phase Flow for $P = 5{\cdot}8$ MPa, $T = 273^\circ$C

Tests were conducted for the following void fraction values: $\beta = 0{\cdot}70$, 0·80, 0·90 and 0·96. Two types of tests were conducted, albeit at the same test conditions. In test type l, the gas velocity j_g was held constant, while the liquid velocity j_l was incremented; as a result, for this test the void fraction changed for each velocity setting. In test type 2, both j_g and j_l were adjusted to maintain the void fraction at a constant value throughout the test. When plotting the final type 1 test results, data for a given void fraction (from tests at several

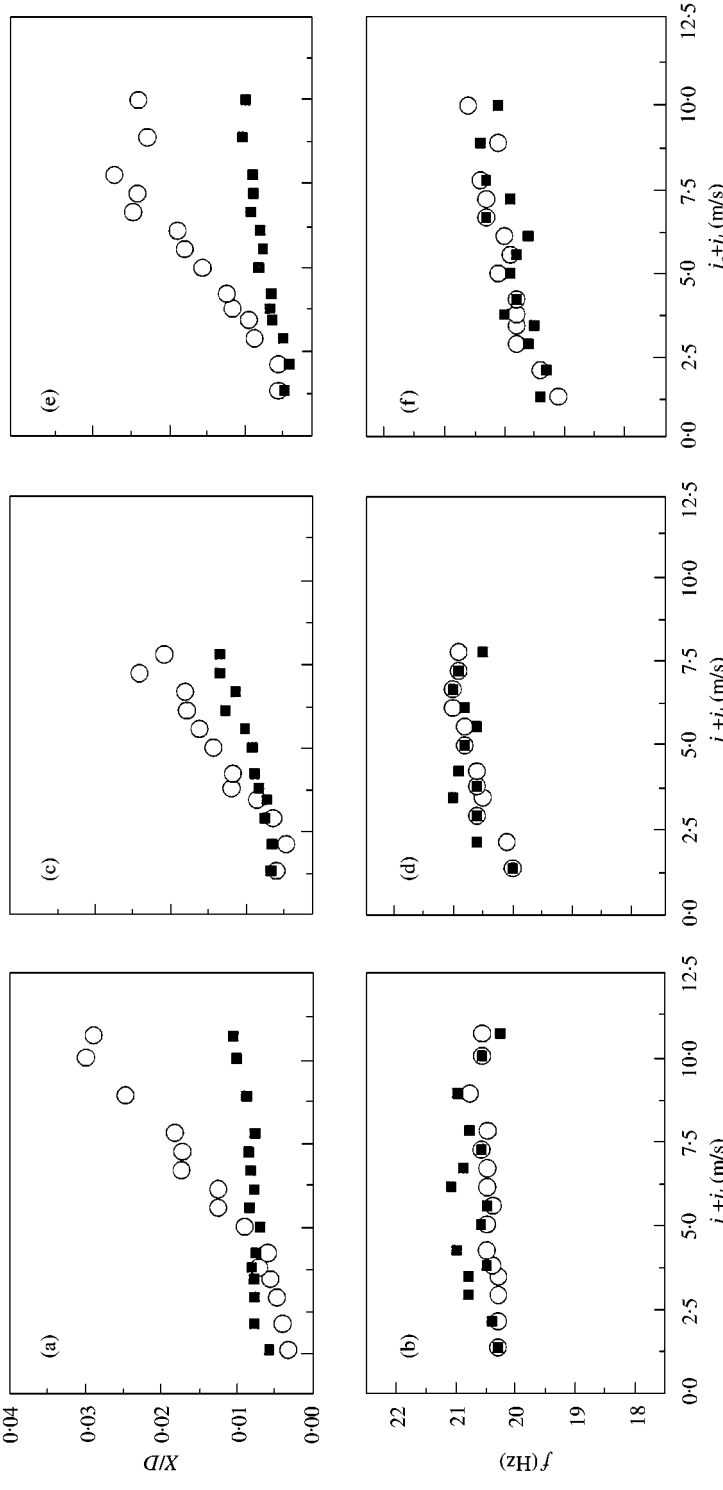

Figure 4. Vibration amplitudes and frequencies for $P = 0{\cdot}5$ MPa, $T = 150°C$, $\beta = 0{\cdot}90$: (a, b) tube S2; (c, d) tube S16; (e, f) tube S29; ■, drag; ○, lift.

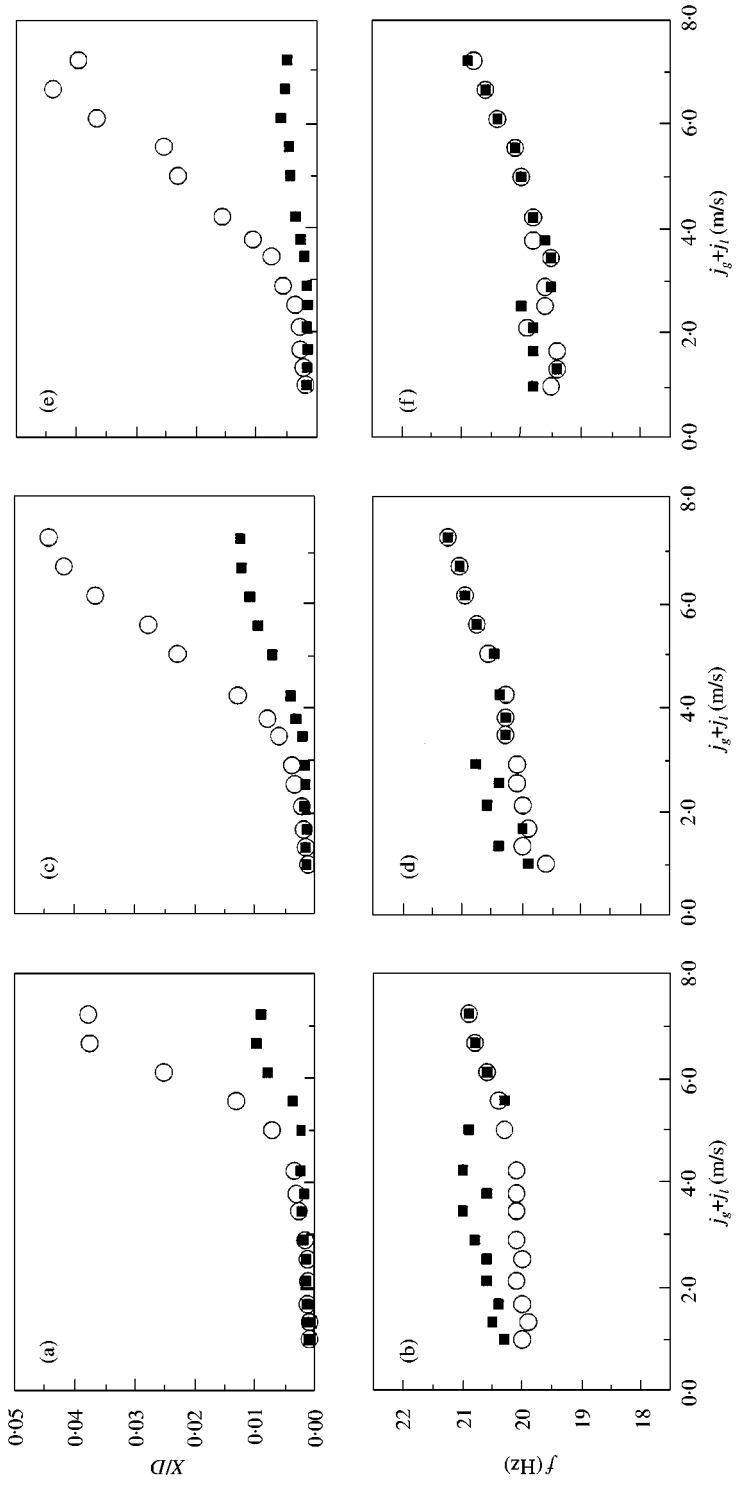

Figure 5. Response amplitudes and frequencies for $P = 3{\cdot}0$ MPa, $T = 230°C$, $\beta = 0{\cdot}90$: (a, b) tube S2; (c, d) tube S16; (e, f) tube S29; ■, drag; ○, lift.

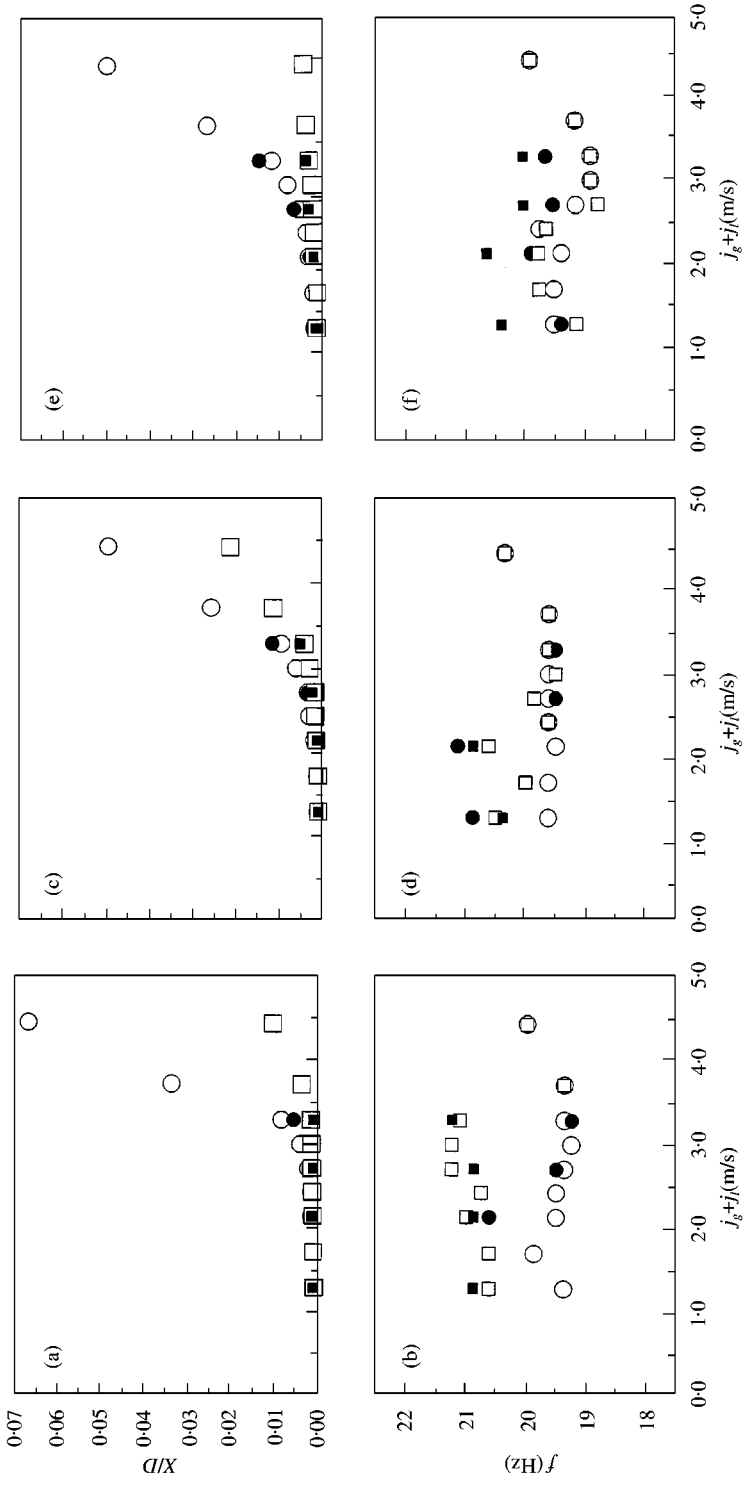

Figure 6. Response amplitudes and frequencies for $P = 5{\cdot}8$ MPa, $T = 273°C$, $\beta = 0{\cdot}70$: (a, b) tube S2; (c, d) tube S16; (e, f) tube S29. Test types 1 and 2 are indicated by filled and open symbols, respectively. ■, □, drag; ●, ○, lift.

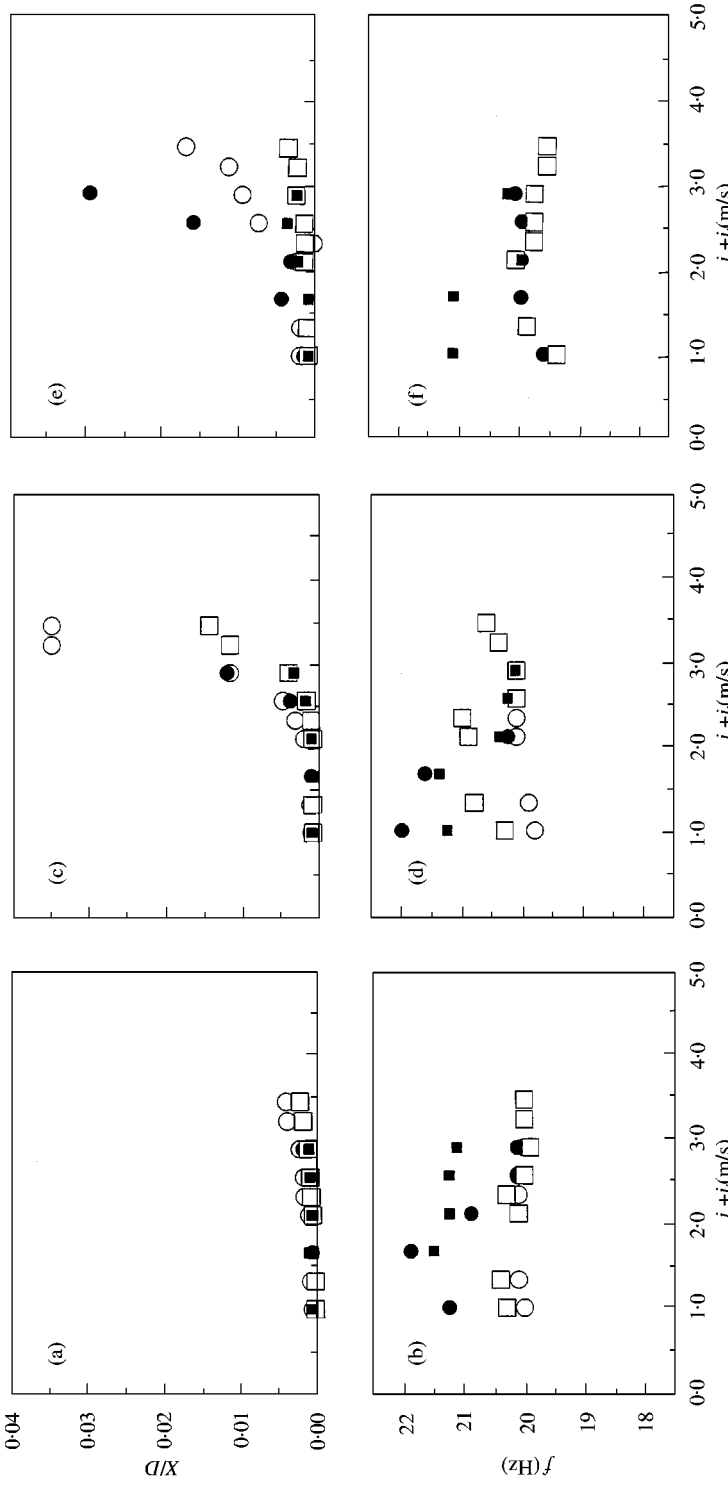

Figure 7. Response amplitudes and frequencies for $P = 5{\cdot}8$ MPa, $T = 273°C$, $\beta = 0{\cdot}90$: (a, b) tube S2; (c, d) tube S16; (e, f) tube S29. Test types 1 and 2 are indicated by filled and open symbols, respectively. ■, □, drag; ●, ○, lift.

$j_g$values) were put together. Direct comparison with type 2 test results could therefore be made.

Figure 6 shows test results for 0·70 void fraction. Tests 1 and 2 are indicated by filled and open symbols, respectively. The two test types also give a measure of the repeatability of the results. The response amplitude graphs show good agreement between the two tests. The frequency plots on the other hand show that, prior to instability, cross-flow frequencies are initially higher for test type 1 (fixed j_g) for tubes S2 and S16; on the other hand, the frequency is slightly lower for tube S29. Following instability, the in-flow motion becomes coupled to the cross-flow motion. Fluidelastic instability occurs in the lift direction for all three tubes. The critical velocities are 2·9, 2·4 and 2·3 m/s for tubes S2, S16 and S29, respectively.

Figure 7 shows test results for $\beta = 0{\cdot}90$. Tube S2 and S16 show good agreement in response amplitudes for the two types of tests. Once again the difference in cross-flow frequencies at low velocities occurs. For tube S29, however, there is a delay in the onset of instability for test 2. The critical velocities are, nevertheless, reasonably close. Instability velocities for this void fraction are 3·0, 2·1 and 2·4 m/s, respectively, for S2, S16 and S29 tubes.

Comparing with instability velocity values for $\beta = 0{\cdot}70$, the change in void fraction does not result in a significant change in the critical velocities. This is attributed to the fact that in both cases, the flow structure remains essentially unchanged [see Part I, Nakamura *et al.* (2002)]. Tests conducted for $\beta = 0{\cdot}80$ and upto $\beta = 0{\cdot}96$ gave closely similar results to the foregoing. Tabulated results for all β values are presented in Tables 3–5.

3.6. Overview of Stability Results at High Temperature and Pressure

The stability results presented in the foregoing are summarized in Figures 8 and 9. In Figure 8, critical velocities for a fixed void fraction $\beta = 0{\cdot}90$ are plotted versus pressure P. On average, the instability velocity decreases as P increases. The instability velocities are also closer for different tubes, as the pressure increases. Figure 9 shows the variation of critical velocity with void fraction for $P = 5{\cdot}8$ MPa ($T = 273^{\circ}$C). An average instability velocity of 3·0 m/s is obtained for this range of void fractions.

Connors' constant K (equation (5)) values are presented in Tables 3–5 while the stability results are plotted in standard dimensionless form in Figure 10. For most of the test data, K is between 3 and 5. Finally, a comparison with other two-phase flow tests is made in Figure 11. The present data fall centrally within other published data. The trend agrees more closely with other steam-water tests, particularly for normal square arrays.

4. COMPARISON WITH THEORY

A brief theoretical analysis of the instability phenomenon is presented in this section. The theoretical basis is a standard, unsteady fluid-dynamics model (Tanaka & Takahara 1981; Chen 1983).

4.1. Unsteady Fluid-Dynamics Model

We consider a tube array in which the forces acting on a given tube are the result of motion of the immediate neighbours as well as the tube itself. For an in-line geometry the representative kernel consists of five tubes as shown in Figure 12. The governing equation for the central tube 1, for instance, is

$$[M_1]\{\ddot{X}_1\} + [C_1]\{\dot{X}_1\} + [K_1]\{X_1\} = \sum_{j=1}^{5} ([A_j]\{\ddot{X}_j\} + [D_j]\{\dot{X}_j\} + [S_j]\{X_j\}), \qquad (6)$$

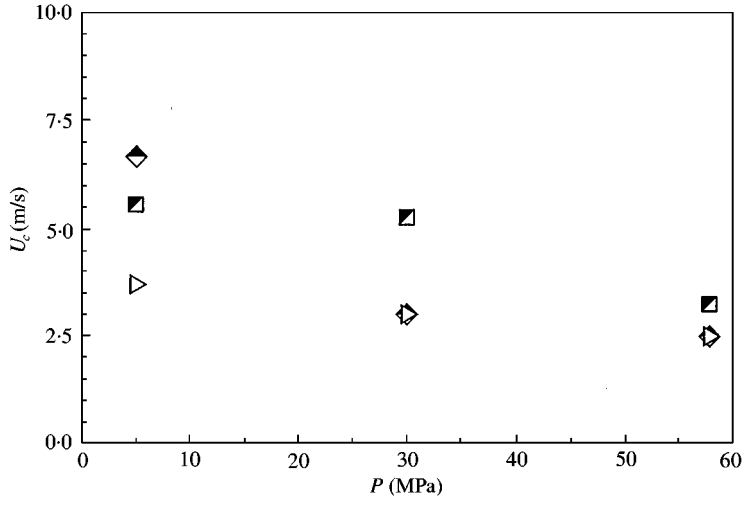

Figure 8. Variation of instability velocity with pressure P (and T), void fraction $\beta = 0{\cdot}90$, for tube: ◩, S2; ▷, S16; ◈, S29, in the lift direction.

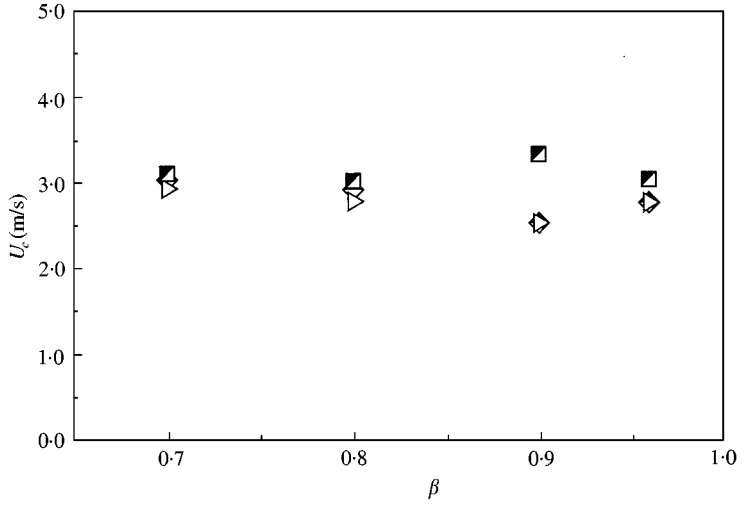

Figure 9. Variation of instability velocity with void fraction β at $P = 5{\cdot}8$ MPa ($T = 273°$C), for tube: ◩, S2; ▷, S16; ◈, S29, in the lift direction.

where $\{X_j\} = \{x_j, y_j\}^{\mathrm{T}}$ is the displacement vector of tube 'j'. $[A]$ $[D]$ and $[S]$ are the fluid-related (added) mass, damping and stiffness matrices; the subscript 'j' indicates the tube whose motion induces the fluid forces. Tube 1 is simply represented as a flexibly mounted rigid body in equation (6). By considering a kernel centred at each of the remaining tubes, equations identical to (6) can be written for the surrounding tubes.

For the purpose of comparison with experimental results, it is sufficient to consider the case of only one moving tube. Furthermore, in view of the fact that instability occurred only in the cross-flow direction, a single-degree-of-freedom model is considered. Equation (6) then simplifies to the following scalar form:

$$m\ddot{x} + c\dot{x} + kx = -a\ddot{x} + d\dot{x} + sx, \quad a > 0, \tag{7}$$

TABLE 3
Row-16 tube stability results

P (MPa)	ρ (kg/m^3)	β	ζ_t% (fluid + structure)	f_n (Hz)	U_c (m/s)	U_c/f_nD	$m\delta/\rho D^2$	K
5·8	249·62	0·70	1·42	19·6	2·4	5·51	0·836	6·03
5·8	176·28	0·80	1·90	19·5	2·4	5·54	1·552	4·45
5·8	102·94	0·90	1·40	20·3	2·1	4·65	1·850	3·42
5·8	58·94	0·96	0·71	20·0	2·0	4·50	1·624	3·53
3·0	95·62	0·90	1·93	19·5	3·2	7·38	2·719	4·48
0·5	93·96	0·90	1·85	20·1	3·0	6·73	2·578	4·19

TABLE 4
Row-2 tube stability results

P (MPa)	ρ (kg/m^3)	β	ζ_t% (fluid + structure)	f_n (Hz)	U_c (m/s)	U_c/f_nD	$m\delta/\rho D^2$	K
5·8	249·62	0·70	2·74	19·3	2·9	6·76	1·614	5·32
5·8	176·28	0·80	1·89	19·5	2·9	6·69	1·547	5·38
5·8	102·94	0·90	1·87	20·0	3·0	6·75	2·466	4·30
5·8	58·94	0·96	1·01	20·1	3·0	6·71	2·310	4·41
3·0	95·62	0·90	3·25	20·0	4·8	10·80	4·589	5·04
0·5	93·96	0·90	3·10	20·3	4·5	9·97	4·317	4·80
0·1	1000	0·00	1·14	17·5	0·75	1·93	0·220	4·11

TABLE 5
Row-29 tube stability results

P (MPa)	ρ (kg/m^3)	β	ζ_t% (fluid + structure)	f_n (Hz)	U_c (m/s)	U_c/f_nD	$m\delta/\rho D^2$	K
5·8	249·62	0·70	2·16	19·2	2·3	5·39	1·272	4·78
5·8	176·28	0·80	2·34	19·3	2·7	6·29	1·910	4·55
5·8	102·94	0·90	2·20	19·2	2·4	5·62	2·907	3·30
5·8	58·94	0·96	1·55	19·2	2·3	5·39	3·543	2·86
3·0	95·62	0·90	2·43	19·2	3·0	7·05	3·432	3·81
0·5	93·96	0·90	3·40	19·1	6·5	15·31	4·738	7·03

where the subscript '1' has been dropped. The coefficients on the *right-hand side* are related to the measured unsteady fluid force coefficient magnitude and phase (Mureithi *et al.* 2002) as follows:

$$a = \frac{1}{2}\rho D^2 C_{ma}, \quad d = \frac{1}{2}\rho DU\bar{C}_f \sin\bar{\phi}_f - c_v - c_{tp},$$

$$s = \frac{1}{2}\rho U^2\left(\bar{C}_f \cos\bar{\phi}_f - \frac{C_{ma}}{(U/D)^2}\right); \tag{8}$$

C_{ma} is the added mass coefficient, c_v the (two-phase) viscous damping and c_{tp} the two-phase damping (Nakamura *et al.* 2002); $\bar{C}_f$ and $\bar{\phi}_f$ are the unsteady fluid force magnitude and phase after elimination of the flow velocity independent components associated with c_v and c_{tp} above (Mureithi *et al.* 2002).

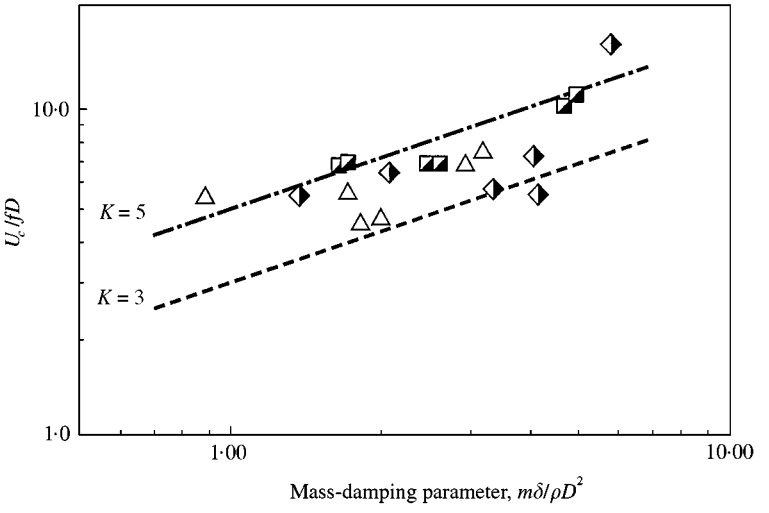

Figure 10. Reduced critical flow velocity versus mass-damping parameter ($P = 0{\cdot}5,3{\cdot}0$ and $5{\cdot}8$ MPa.) for tube: ◪, S2; △, S16; ⬗, S29 in the lift direction.

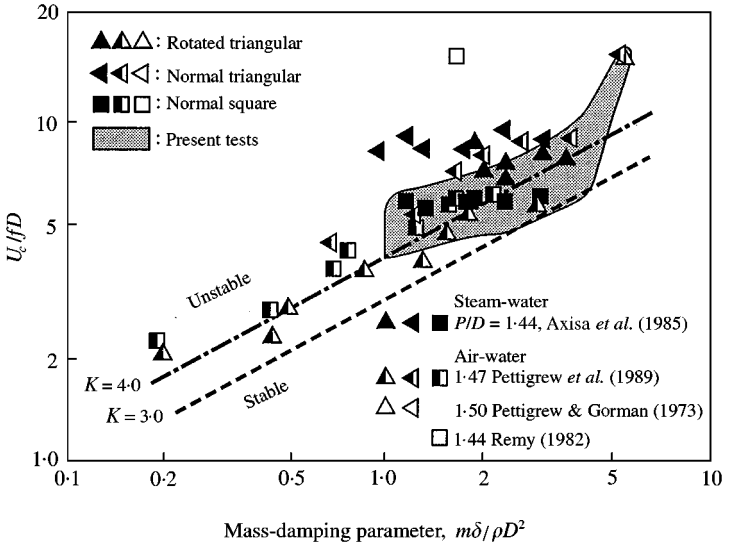

Figure 11. Comparison of present data with previously published data taken from Pettigrew & Taylor (1994).

To solve equation (7), the following vector is introduced:

$$\{Z\} = [\dot{x}, x]^{\mathrm{T}}. \tag{9}$$

Considering a solution

$$\{Z(t)\} = \{Z_0\}e^{\lambda t}, \tag{10}$$

equation (7) can be converted to the following standard eigenvalue problem:

$$[\lambda P + Q]\{Z_0\} = \{0\}, \tag{11}$$

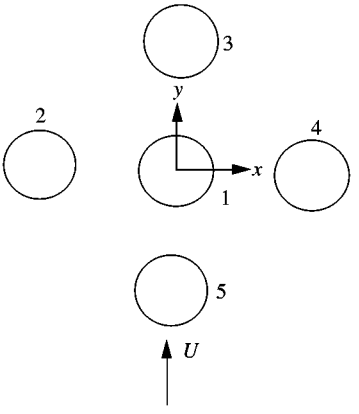

Figure 12. Tube array kernel for unsteady fluid-dynamic model.

where

$$[P] = \begin{bmatrix} 0 & \bar{m} \\ \bar{m} & \bar{c} \end{bmatrix}, \qquad [Q] = \begin{bmatrix} -\bar{m} & 0 \\ 0 & \bar{k} \end{bmatrix}, \tag{12}$$

$$\bar{m} = m + \frac{1}{2}\rho D^2 C_{ma}, \qquad \bar{c} = c - \frac{1}{2}\rho DU\bar{C}_f \sin\bar{\phi}_f + c_v + c_{tp},$$

$$\bar{k} = k - \frac{1}{2}\rho U^2\left(\bar{C}_f \cos\bar{\phi}_f - \frac{C_{ma}}{(U/D)^2}\right) \tag{13}$$

The matrices $[P]$ and $[Q]$ in equation (12) are functions of U (among other parameters) through $\bar{C}_f$ and $\bar{\phi}_f$. In Part II of the study it was found that C_f and ϕ_f (hence, $\bar{C}_f$ and $\bar{\phi}_f$) are in general multiple-valued functions of the reduced velocity U/fD. One is therefore faced with a dilemma of choice of $\bar{C}_f$ and $\bar{\phi}_f$ when constructing the $[P]$ and $[Q]$ matrices.

Fortunately for the case of a single flexible tube this problem can be overcome. $\bar{C}_f$ and $\bar{\phi}_f$ have two branches for tube S16 for $P = 5{\cdot}6$ MPa (Mureithi *et al.* 2002). Along the lower $\bar{\phi}_f$ branch, the phase angle is in the range $-180 < \bar{\phi}_f < 0$ for all values of U/fD. Consequently, only positive damping is induced in view of equation (13). For the stability analysis then it suffices to consider only the upper branch of $\bar{\phi}_f$, as shown in Figure 13; the corresponding $\bar{C}_f$ branch, in Figure 13(b), is the lower one. A fourth-order polynomial fit performed on the data is shown with solid lines in Figure 13. This approach yields a conservative stability boundary.

4.2. Theoretical Stability Boundary and Comparison with Experiments

Results of a stability analysis of lift direction motion of the test tubes are shown in Figure 14. Tube parameters are those given in Table 1 while flow conditions were a high pressure ($P = 5{\cdot}6$ MPa) and a void fraction of $\beta = 0{\cdot}9$.

Comparison of the predicted stability boundary is made with experimental data for $P = 3{\cdot}0$ MPa, $\beta = 0{\cdot}90$ and $P = 5{\cdot}8$ MPa, $\beta = 0{\cdot}90$–$0{\cdot}96$ ($\beta = 0{\cdot}70$–$0{\cdot}80$ data are also included for tube S16). The overall agreement is reasonably good. In the case of $P = 5{\cdot}8$ MPa, $\beta = 0{\cdot}90$, where vibration and unsteady fluid forces data are closely matched for tube S16, the critical velocity is accurately predicted as seen in the figure; data corresponding to $P = 5{\cdot}8$ MPa, $\beta = 0{\cdot}90$ are shown with larger symbols. The good agreement with tube S29

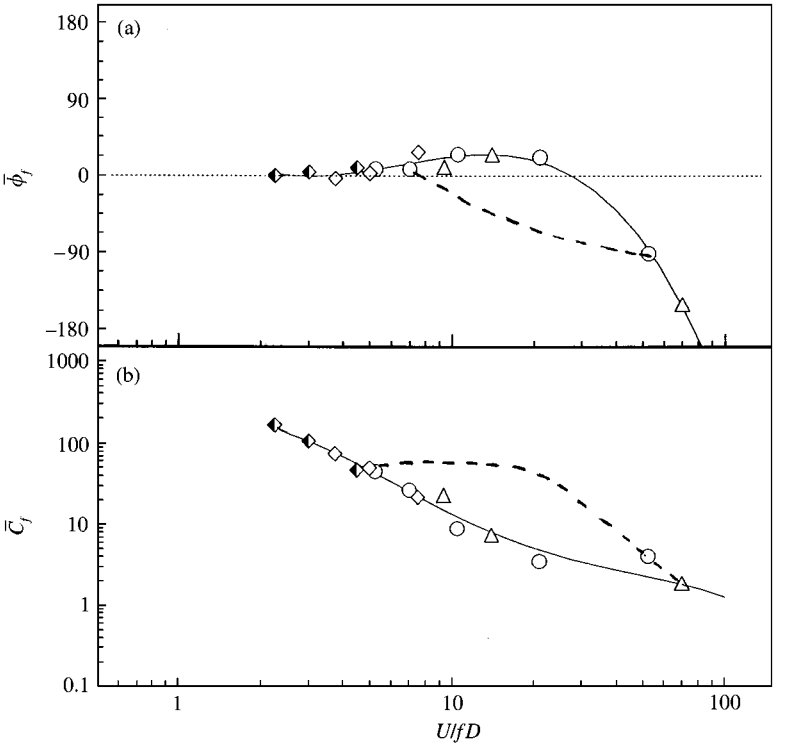

Figure 13. Conservative branch (solid line) of tube S16 adjusted fluid force coefficient used in stability analysis for $P = 5{\cdot}6$ MPa: (a) phase, (b) magnitude. Data shown are for phase velocities ((j_g, j_l): ◐, (0·10, 0·9); ◇, (0·17, 1·5); ○, (0·23, 2·1); and △, (0·31, 2·8) m/s.

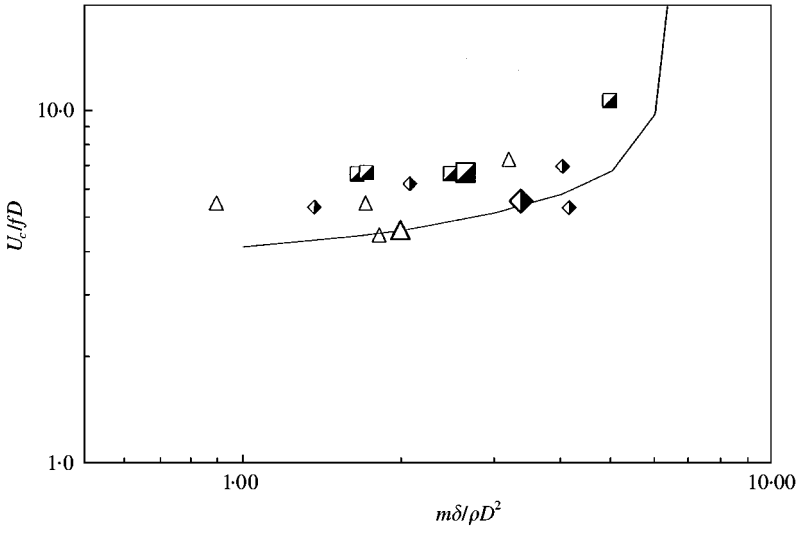

Figure 14. Predicted instability boundary for tube S16 ($P = 5{\cdot}6$ MPa, $\beta = 0{\cdot}90$) compared with experimental data for tubes: ◪, S2; △, S16; ◑, S29; $P = 3{\cdot}0$ MPa, $\beta = 0{\cdot}90$ and $P = 5{\cdot}8$ MPa, $\beta = 0{\cdot}70$–$0{\cdot}96$. Data for $P = 5{\cdot}8$ MPa, $\beta = 0{\cdot}90$ are indicated by larger symbols.

data indicates close similarity between fluid forces within and downstream of the array. Entrance effects at row 2, on the other hand, have a stabilizing effect.

The sharply rising trend in the instability velocity for $m\delta/\rho D^2 > 4$ is the result of a change in the phase difference between the fluid force and tube displacement. As seen in Figure 13, $\bar{\phi}_f$ plateaus starting near $U/fD = 8$. Data for triangular arrays (Pettigrew & Gorman 1973; Pettigrew *et al.* 1989) shows a similar stabilizing trend as seen in Figure 11. This effect may therefore be intimately associated with two-phase flow, rather than a particular array geometry.

Finally, data at 0·5 MPa has not been considered in the analysis. It is necessary to consider nonstationarity effects in this case. This is beyond the intended scope of the present series of papers. It should be remarked, however, that although an analysis based on homogeneous flow conditions gives an apparently conservative stability boundary for this case also, this may (only) be the absolute instability boundary. Nakamura et al. (1995) have shown theoretically that intermittent instability precedes absolute instability. Unacceptably large vibration amplitudes may occur intermittently. The effect of nonstationarity should therefore be incorporated in any theoretical analysis.

CONCLUSIONS

The vibration response of a flexibly mounted tube in an in-line array has been investigated. Possibly due to the high Reynolds number in liquid flow at high-pressure, flow periodicity resonance did not occur. In two-phase flow, the location near the array entrance was more stable than deep within or downstream of the array. In homogeneous (high pressure/temperature) flow, fluidelastic instability was similar to the same phenomenon in single-phase flow. Intermittent instability, on the other hand, occurred in nonhomogeneous flow, as confirmed by the measured unsteady fluid forces. For $P = 5{\cdot}8$ MPa, the instability velocity varied little with void fraction in the range $\beta = 0{\cdot}70$–$0{\cdot}96$. This is attributed to the invariance in flow pattern over this range of void fraction.

A theoretical analysis showed that fluidelastic instability in homogeneous or nearly homogeneous two-phase flows can be predicted with reasonable accuracy. Matters are, however, quite different for nonhomogeneous flow where a new approach is needed.

CLOSING REMARKS

The aim of the present study was two-fold. Firstly, to obtain data at steam generator prototypical operating conditions. Secondly, to perform a preliminary theoretical investigation of the phenomenon of fluidelastic instability in two-phase flow, employing the measured experimental data.

In Part I of this series, two-phase damping and fluid added mass were presented. Using controlled tube excitation and sophisticated time-domain identification techniques, accurate damping results were obtained. Drag-direction damping was found to be high. Tubes located deep in the array had the lowest damping. Damping and added mass results were in good agreement with previously reported data.

Unsteady fluid dynamic forces were the subject of Part II of the study. Significant differences from the case of single-phase flow were discovered. Two-phase damping comprised a significant component of the total fluid-induced damping. Most remarkable was the multivalued nature of the fluid force coefficients when expressed as functions of reduced flow velocity. The force coefficients associated with a tube's own motion could be approximated by a function with two branches for the higher pressure $P = 3{\cdot}0$ and $5{\cdot}6$ MPa conditions. Less clear was the form of intertube coupling-related forces. The low coherence associated with intertube coupling reduces the probability of the *initiation* of a coupled (intertube) mode instability.

For nonhomogeneous flow ($P = 0{\cdot}5$ MPa), a time–frequency analysis confirmed that the instantaneous force–displacement transfer function was strongly time dependent. This provides an explanation for the existence of intermittent instability.

The results of vibration tests coupled with a theoretical stability analysis were presented in Part III of this paper. For single-phase liquid flow at high pressure, flow periodicity resonance, observed at atmospheric pressure (0·1 MPa) did not occur. This was related to the increase in Reynolds number at the transition region, weakening the flow periodicity mechanism.

Fluidelastic instability occurred at all two-phase flow test conditions. In homogeneous flow, instability was clear and well defined. In nonhomogeneous flow, turbulence and intermittency obscured the appearance of clear instability. In all cases, instability occurred in the lift direction.

A theoretical analysis of the instability mechanism was performed employing the measured unsteady fluid forces reported in Part II of the study. The complexity of the functional relation between the force coefficients and reduced flow velocity poses some difficulties in applying the force coefficients. For the case of a single flexible tube it was possible to perform a conservative stability analysis by selecting the destabilizing branch of the fluid force. A much more involved analysis would be needed for the case of a flexible bundle. The predicted stability boundary for a single flexible tube agreed reasonably well with test data both for the simulated internal array location as well as other locations. The second-row tube was marginally more stable than the internal- and downstream-located tubes in homogeneous flow.

Stability prediction in the case of nonstationary flow conditions requires further work. The importance of such an analysis was highlighted by the potential occurrence of intermittent instability, which cannot be predicted by the present analysis based on a steady-flow assumption.

In closing, it is gratifying to find that ideas based on the analysis of stability in single-phase flow are to a reasonable extent applicable in the case of homogeneous two-phase flow. Such an analysis is, however, based on the assumption of stationarity and perfect coherence. Nonstationarity needs to be considered for a better understanding of intermittent instability. Data obtained in this study indicate that there is low coherence between neighbouring tubes for small displacement amplitudes. The analysis of coupled (intertube) mode instability should therefore give results in terms of probability of instability due to the imperfect correlation. With regard to the initiation of instability, it would appear that forces associated with the tube motion itself are the prime candidates, rather than intertube coupling forces. This is suggested by the poor intertube correlation presented in Part II of this series of papers. Further supporting evidence has recently been presented by Nakamura *et al.* (1999) where, for the same array geometry (in freon two-phase flow), the number of flexible tubes had little effect on the instability threshold. This, however, is not the case for *triangular* geometries, as shown by Pettigrew *et al.* (1995). For in-line geometries, it would seem that single flexible tube models may still have "*something to say*" about the overall array dynamics, particularly with respect to the onset of instability. Post-instability dynamics, on the other hand, may be expected to involve coupled motions as large vibration amplitudes increase intertube force correlations.

ACKNOWLEDGEMENTS

Experimental apparatus assembly, pretesting, sensor calibration and actual testing were primarily performed by K. Mitsumori. The authors gratefully acknowledge his expert work.

This work was jointly financed by Mitsubishi Heavy Industries and the five electric power companies operating PWRs in Japan (Kansai Electric, Shikoku Electric, Kyushu Electric, Hokkaido Electric and Japan Atomic Power Company).

References

Axisa, F., Boheas, M. A. & Villard, B. 1985 Vibration of tube bundles subjected to steam-water cross-flow: a comparative study of square and triangular arrays. Paper B1/2, 8*th International Conference on Structural Mechanics in Reactor Technology*, Brussels, Belgium.

Chen, S. S. 1983 Instability mechanisms and stability criteria of a group of circular cylinders subjected to cross flow; I: Theory. *ASME Journal of Vibration, Acoustics, Stress, and Reliability in Design* **105**, 51–58.

Chen, S. S. 1987 *Flow-Induced Vibration of Cylindrical Structures.* Washington, D. C.: Hemisphere Publishing.

de Langre, E., Villard, B. & Entenmann, K. 1995 A spectrum of two-phase flow random forces in tube arrays. In *Flow Induced Vibration* (ed. P. W. Bearman), pp. 107–117. Rotterdam: A. A. Balkema.

Feenstra, P. A., Judd, R. L. & Weaver, D. S. 1995 Fluidelastic instability in a tube array subjected to two-phase R-II cross-flow. *Journal of Fluids and Structures* **9**, 747–771.

Gay, N., Decembre, P. & Launay, J. 1988 Comparison of air–water to water-freon two-phase cross flow effects on vibratory behaviour of a tube bundle. *Flow Induced Vibration and Noise in Cylinder Arrays* (eds M. P. Paidoussis, S. S. Chen & M. D. Bernstein), Vol. 3, pp. 139–158. New York: ASME.

Heilker, W. J. & Vincent, R. Q. 1981 Vibration in nuclear heat exchangers due to liquid and two-phase flow. *ASME Journal of Engineering for Power* **103**, 358–366.

Hirota, K., Nakamura, T., Mureithi, N. W., Kasahara, J., Kusakabe, T. & Takamatsu, H. 1996 Dynamics of an in-line tube array in steam–water flow; Part III: Fluidelastic instability tests and comparison with theory. In *Flow-Induced Vibration* 1996 (ed. M. J. Pettigrew) , PVP Vol. 328, pp. 123–134. New York: ASME.

Marn, J. & Catton, I. 1992 On the instability of two-phase cross flow through a staggered cylinder array. In *Cross-Flow Induced Vibration of Cylinder Arrays* (eds M. P. Paidoussis, Chen, S. S. & D. A. Steininger), Vol. 2; PVP-Vol. 242, pp. 57–68. New York: ASME.

Mureithi, N. W., Nakamura, T., Hirota, K., Murata, M., Utsumi, S., Kusakabe, T. & Takamatsu, H. 2002 Dynamics of an in-line tube array subjected to steam–water cross-flow; Part II: Unsteady fluid forces. *Journal of Fluids and Structures* **16**, 137–152.

Nakamura, T., Fujita, K., Kawanishi, K., Yamaguchi, N. & Tsuge, A. 1995 Study on the vibrational characteristics of a tube array caused by two-phase flow; Part II: Fluidelastic vibration. *Journal of Fluids and Structures* **9**, 539–562.

Nakamura, T., Hirota, K., Tomomatsu, K., Kasahara, J. & Takamatsu, H. 1999 On positional effect of flexible tubes in a square array subjected to freon two-phase flow. In *Flow Induced Vibration* (ed. M. J. Pettigrew), PVP-Vol. 389, pp. 73–80. New York: ASME

Nakamura, T., Mureithi, N. W., Hirota, K., Murata, M., Utsumi, S., Kusakabe, T. & Takamatsu, H. 2002 Dynamics of an in-line tube array subjected to steam-water cross-flow; Part I: Two-phase damping and added mass. *Journal of Fluids and Structures* **16**, 123–136.

Pettigrew, M. J. & Gorman, D. J. 1973 Experimental studies on flow-induced vibration to support steam generator design; Part III: Vibration of small tube bundles in liquid and two-phase cross flow. Paper No. 424, *International Symposium on Vibration Problems in Industry*, Keswick, U. K.

Pettigrew, M. J., Tromp, J. H., Taylor, C. E. & Kim, B. S. 1989 Vibration of tube bundles in two-phase cross flow; Part II: Fluidelastic instability. *ASME Journal of Pressure Vessel Technology* **111**, 478–487.

Pettigrew, M. J. & Taylor, C. E. 1994 Two-phase flow-induced vibration: An overview. *ASME Journal of Pressure Vessel Technology* **116**, 233–253.

Pettigrew, M. J., Taylor, C. E., Jong, J. H. & Currie, I. G. 1995 Vibrations of a tube bundle in freon two-phase cross-flow. *ASME Journal of Pressure Vessel Technology*, **117**, 321–329.

Remy, F. N. 1982 Flow induced vibration of tube bundles in two-phase cross flow. In *Proceedings of the 3rd International Conference on Vibration in Nuclear Plants*, Paper No. 1.9, Vol. 1, pp. 135–160.

TANAKA, H. & TAKAHARA, S. 1981 Fluidelastic vibration of tube array in cross-flow. *Journal of Sound and Vibration* **77**, 19–37.

WEAVER, D. S. & ABD RABBO, A. 1985 A flow visualization study of a square array of tubes in water crossflow. *ASME Journal of Fluids Engineering* **107**, 354–363.

ZIADA, S. & OENGÖREN, A. 1992 Vorticity shedding and acoustic resonance in an in-line tube bundle; Part I: Vorticity shedding. *Journal Fluids and Structures* **6**, 271–292.